Parity violation in neutron resonances of ^{117}Sn

D. A. Smith,[1,*] J. D. Bowman,[1] B. E. Crawford,[2,†] C. A. Grossmann,[3] T. Haseyama,[4] Mikkel B. Johnson,[1] A. Masaike,[4,‡] Y. Matsuda,[4,§] G. E. Mitchell,[3] V. A. Nazarenko,[5] S. I. Penttila,[1] N. R. Roberson,[2] S. J. Seestrom,[1] E. I. Sharapov,[6] L. M. Smotritsky,[5] S. L. Stephenson,[3,†] S. Tomsovic,[7] and V. W. Yuan[1]

[1]*Los Alamos National Laboratory, Los Alamos, New Mexico 87545*

[2]*Duke University, Durham, North Carolina 27708*
and Triangle Universities Nuclear Laboratory, Durham, North Carolina 27708-0308

[3]*North Carolina State University, Raleigh, North Carolina 27695-8202*
and Triangle Universities Nuclear Laboratory, Durham, North Carolina 27708-0308

[4]*Physics Department, Kyoto University, Kyoto 606-01, Japan*

[5]*Petersburg Nuclear Physics Institute, RU-188350 Gatchina, Russia*

[6]*Joint Institute for Nuclear Research, RU-141980 Dubna, Russia*

[7]*Department of Physics, Washington State University, Pullman, Washington 99164-2814*

(Received 17 February 2000; revised manuscript received 19 April 2001; published 19 June 2001)

Parity nonconservation (PNC) has been studied in neutron *p*-wave resonances of ^{117}Sn. The longitudinal asymmetries were measured for 29 *p*-wave resonances in the neutron energy range 0.8 eV to 1100 eV. Statistically significant PNC effects were observed for four resonances. A statistical analysis determined the rms weak mixing matrix element and the weak spreading width. A weak spreading width of $\Gamma_w = (0.28^{+0.56}_{-0.15}) \times 10^{-7}$ eV was obtained for ^{117}Sn.

DOI: 10.1103/PhysRevC.64.015502 PACS number(s): 25.40.Ny, 24.80.+y, 11.30.Er, 27.90.+b

I. INTRODUCTION

The observation of very large parity nonconserving (PNC) effects in neutron resonances [1] initiated an extensive study of parity violation in nuclei. For some *p*-wave resonances at low energies the helicity dependence of the neutron cross section is strongly enhanced and shows very large PNC asymmetries. These large effects are the result of mixing of neighboring *s*-wave resonances with the *p*-wave resonances in question. This effect was first predicted by Sushkov and Flambaum [2] and observed shortly thereafter by Alfimenkov *et al.* [1]. Also a new approach of the data analysis was developed where the compound nucleus is treated as a statistical system and the PNC matrix elements are assumed to be independent random Gaussian variables. This approach can be compared with the classic approach of measuring a parity-forbidden observable related to parity doublets in light nuclei [3]. There the major difficulty was determination of the wave functions of the states with sufficient precision, while in the present approach the primary difficulty is obtaining sufficient PNC effects to perform a statistical analysis and sufficient spectroscopic information to reduce the size of the error in the determination of the relevant parameters.

The TRIPLE Collaboration built an experimental system to measure many PNC asymmetries in the neutron resonances of a given nuclide, in order to perform a statistical analysis. These measurements and their analysis have been discussed in a number of reviews [4–6]. Following initial measurements in ^{238}U [7] and ^{232}Th [8], we redesigned and rebuilt the entire experimental system and repeated with much higher statistics the study of these two nuclides [9,10]. Many PNC effects were observed and rms weak matrix elements and weak spreading widths were determined. It was considered important to extend these measurements to other regions of the nuclear periodic table. Since the study of the PNC effects on *p*-wave resonances is practical only in the region of a maximum of the *p*-wave strength function, we next performed experiments in the region $A = 90$–130, near the $3p$ strength function maximum at $A = 110$. Our collaboration has performed measurements on ^{93}Nb [11], ^{103}Rh [12], ^{106,108}Pd [13], ^{107,109}Ag [14], ^{113}Cd [15], ^{115}In [16], ^{121,123}Sb and ^{127}I [17], and ^{133}Cs [18].

The ^{117}Sn target has a special feature that makes the study of parity violation more interesting—the ^{117}Sn nucleus has a closed proton shell (at $Z = 50$ the $1g_{9/2}$ shell is filled). The excitations of the compound system ^{118}Sn produced in the neutron capture are dominated by couplings of multiparticle-multihole valence neutron configurations. As a result, the matrix elements of the two-body part of the weak isovector pion-nucleon exchange potential are expected to be zero and a theoretical treatment of the parity violation simplifies.

The fact that the target ^{117}Sn has nonzero spin I leads to a number of complications in the analysis. The parity violation is caused by the mixing of *s*-wave resonances into *p*-wave resonances. However, only those *s*-wave resonances with the same total spin J but with opposite parity as a given *p*-wave resonance can mix to produce parity violation. For an even-even nuclide with $I = 0$ all of the *s*-wave resonances have the

*Present address: Stanford Linear Accelerator Center, Stanford, CA 94309.

†Present address: Gettysburg College, Gettysburg, PA 17325.

‡Present address: Fukui University of Technology, 3-6-1 Gakuen Fukui-shi, Japan.

§Present address: Institute of Physical and Chemical Research (RIKEN), Saitama 351-0198, Japan.

same spin $J=\frac{1}{2}$, and the mixing takes place only between $\frac{1}{2}^+$ and $\frac{1}{2}^-$ resonances. When the target nucleus does not have $I=0$, there are two J values for the s-wave resonances and three or four J values for the p-wave resonances. In most cases the spins J are not known. The analysis procedure that we adopt is to include all available spectroscopic information and average over unknown spectroscopic parameters. This increases both the complexity of the analysis and the resulting uncertainty in the determination of the value of the weak matrix element and the weak spreading width.

In Sec. II we describe the experimental procedure. The data processing and analysis are discussed in Sec. III. The determination of the rms weak matrix element and the weak spreading width is presented in Sec. IV. The final section gives a brief summary.

II. EXPERIMENTAL PROCEDURE

The experiment was performed at flight path 2 of the Manuel Lujan Neutron Scattering Center. Neutrons were created via the spallation process: the 800-MeV pulsed proton beam from the Los Alamos Neutron Science Center linac was accumulated in a proton storage ring and then bombarded a tungsten spallation target [19]. The proton pulse is produced at a frequency of 20 Hz, with a time width of 250 ns at the base of the pulse. The resulting neutrons were moderated in a water moderator. After the moderator, the neutrons were collimated to a 10-cm diameter beam inside the 5-m thick biological shield. The neutron energy was determined from the time-of-flight over a 59-m flight path from source to detector. The detector was an array of 24 CsI crystals [20,21] placed around the sample, providing approximately 3.0π of detection solid angle, for detection of gamma rays from neutron capture. These crystals were packed tightly in a cylindrical array, with a 20-cm cylindrical hole through the middle to allow access for the neutron beam and a hollow cylinder of ^{6}Li-loaded polyethylene as a shield. Additional collimators provided a beam spot of 9 cm in diameter at the target. The signals from the CsI crystals were detected with photomultiplier tubes, discriminated using constant fraction discriminators, and fed into a coincidence logic unit as described in Ref. [21]. An event was accepted only if the summed logic pulse resulted from the coincidence of at least two γ-ray signals from the detector array. This requirement reduced the background significantly and provided approximately 50% efficiency of registering the neutron capture event. The output pulses from the coincidence logic unit were counted by a multiscaler and introduced into the data-acquisition system with an accumulating memory and a dwell time of either 0.1 μs or 1 μs. The start time of the time-of-flight spectrum is obtained from the proton pulse, and the resulting time-of-flight covered either 0.8192 ms or 8.192 ms for the 0.1-μs or the 1.0-μs dwell times, respectively. The data were analyzed in the energy interval from 27 eV to 1100 eV for the 0.1-μs dwell time and from 0.8 eV to 300 eV for the 1.0-μs dwell time.

The relative neutron flux for each proton pulse was monitored with a pair of helium ionization chambers [23]. The first chamber contains ^{3}He. Neutron capture on ^{3}He produces a large ionization signal, but background γ rays are also detected. Since there is a large background of γ rays produced by the moderator, a second ionization chamber of the same size and pressure, but containing ^{4}He, was located directly behind the ^{3}He chamber. Since the second ionization chamber is sensitive only to γ rays, the final monitor signal was obtained by subtracting the ^{4}He detector signal from the ^{3}He detector signal. The monitor was necessary for the asymmetry measurements, since large changes in neutron flux between two proton pulses can produce a false asymmetry. The monitor measures the current with accuracy better than 10^{-4} during one run.

The neutron beam was polarized by transmission through a polarized proton target [24,25]. For neutrons scattering from polarized protons, there is a large difference in the cross section for the two neutron helicity states. The transmitted neutron beam was approximately 70% polarized. The polarized protons were produced in frozen ammonia by dynamic nuclear polarization. The ammonia was cooled in liquid ^{4}He to 1 K and placed within a 5-T superconducting magnet. By choice of the microwave frequency the proton polarization state could be changed. Changing the direction of the proton polarization (and therefore of the neutron spin state) provides an excellent opportunity to test for systematic errors. However, since this change took several hours, the polarization state of the target was changed only twice during the experiment.

The neutron polarization was reversed on a short time scale with a system of longitudinal and transverse magnetic fields—a neutron spin flipper [26]. The longitudinal fields are parallel to the beam momentum for the first half of the device and antiparallel for the second half. The transverse field has its maximum at the center of the spin flipper, and when on produces a magnetic field that smoothly reverses direction over the length of the system. The net result is a magnetic field that is constant in magnitude and rotates 180° over the length of the spin flipper. The neutron spin adiabatically follows the direction of the magnetic field and this leads to the reversal of the neutron polarization. When the transverse field is off, the change in the sign of the magnetic field in the center of the spin flipper is too abrupt for the neutron spin to follow the field, and the polarization state remains unchanged. The neutron spin state was reversed every 10 s.

The neutron spin state was changed following an eight-step sequence. The sequence used was: $0++0-00-$, where 0 corresponds to the spin parallel to the beam direction, and $\pm$ corresponds to the spin antiparallel to the beam direction ($\pm$ means that the transverse field is on in the up or down direction). By changing the spin every 10 s, the experiment was insensitive to long time period drifts in the neutron flux or detector efficiency. The use of the eight-step sequence also removed linear or quadratic short term drifts in the count rates. As an additional quality control, each eight-step sequence was labeled good or bad (and stored separately), depending on whether or not the neutron beam monitor varied more than 8% in intensity over the course of the sequence. At the end of each half hour the accumulated

spectra for the good and bad data were stored and labeled as a ''run.''

For low energy neutrons and the long flight distance of 59 m, interaction of the neutron spin with the earth's magnetic field can produce significant depolarization. The neutron polarization was maintained over the flight path from the neutron source to the interaction target with a 10-G solenoidal magnetic field. The entire length of the beam pipe, from the spin flipper to the target, was wrapped in wire coils with a constant electric current as described in Refs. [21,22]. The neutron polarization at the target was monitored by measurement of the well known parity violation in the 0.74-eV resonance in ^{139}La [27]. A lanthanum metal sample was placed behind the interaction target, and a ^{6}Li-loaded glass detector measured the neutron transmission through the ^{139}La sample for two helicity states [28]. This method provided approximately a 20% measurement of neutron polarization per 30-min run to monitor the preservation of the neutron polarization by the spin transport system.

The target was an 87.6% enriched ^{117}Sn solid metal target, in the form of a rectangle of 7.7 cm$\times$6.3 cm on average and 1.3-cm thick. The target was placed in the center of the two CsI arrays, where the normal to the larger target surface was along the beam direction.

III. DATA ANALYSIS

The first step in the analysis was to sort the data into acceptable and unacceptable data runs. As mentioned above, the acquisition system automatically sorted the runs into ''good'' and ''bad'' runs according to the 8% beam stability criterion. Only the ''good'' runs were included to the final analysis. During the ^{117}Sn measurements, however, the beam instability below the 8% threshold produced, from time to time, intensities that were slightly different in flipped and nonflipped parts of some runs. We decided to use the gamma detector signal as a sensitive monitor for such instabilities. The integrated time-of-flight rates of the detector are dominated by counts from strong *s*-wave resonances. Parity violation in these *s*-wave resonances is strongly suppressed to a level less than 10^{-4}. A data run was rejected if the asymmetry in the integrated time-of-flight spectrum was greater than 0.06%. Altogether, this led to rejection of about 7% of the ''good'' runs. The acceptable runs were then summed to obtain the experimental time-of-flight spectrum for each spin state. In the final summed spectra, there was a 0.003% asymmetry for the entire time-of-flight spectrum for both the 0.1-μs and 1.0-μs dwell time data sets.

The summed spectra for each spin state were analyzed with a fitting code FITXS [29] developed specifically for these experiments. FITXS minimizes χ^2 for a region of the time-of-flight spectrum to determine experimental parameters (flight path length, spectrum offset) and resonance parameters (resonance energy, neutron width, γ-ray width). The neutron cross sections were calculated with the formalism of Reich and Moore [30], which provides a description of the resonance shapes for the neutron capture peaks. These resonance shapes were convoluted with an additional width due to Doppler broadening, which is determined by the neutron energy and the target temperature. These Doppler-broadened resonances were then convoluted with the beam response function. The beam response shape was primarily defined by the neutron moderator. The initial beam response function was Gaussian convoluted with an exponential tail. A detailed analysis of the resonance shapes observed in capture and transmission measurements determined that a second Gaussian with a longer exponential tail was required in order to fit the resonance line shape well [9]. The CsI detector did not add any measurable broadening to the line shape. The neutron flux followed a power law of the form $CE^{-\alpha}$. This power law works very well in describing the neutron flux from the moderator for neutron energies from 1 eV to several keV. Since there were no resonances below 1 eV in the present experiment, this expression was used in all of our analyses, and the values of the parameters can be found in Ref. [31]. The CsI detector had a time-of-flight dependent background. This background was fit separately as a quadratic function in each time-of-flight region and then subtracted.

Once the spectral line shapes were understood, the analysis could proceed. The first step was to determine the flight path length and the constant spectrum offset by calibrating to the energies of known resonances. The results are reported in our paper on the neutron spectroscopy of ^{117}Sn [31], which contains other details concerning the data analysis, including multiple scattering corrections and procedures for obtaining the neutron flux parameters, the resonance parameters, and the average level spacings and neutron strength functions. The resonance neutron widths were determined for neutron energies from 1 eV to 1500 eV. The parity of the resonances was inferred from the neutron widths by applying Porter-Thomas distributions in a Bayesian analysis, as described in Ref. [31].

After the neutron resonance energies and widths were obtained, the yield asymmetries were determined for the resonances. The background, resonance energy, and neutron width were held fixed, and the peak area was allowed to vary for each neutron spin state. The yield asymmetries were obtained from the difference between the yields for the two spin states divided by the sum of the yields. The beam polarization was determined by comparing the transmission measurement on ^{139}La to the previously known parity violating asymmetry in the 0.74-eV resonance—$p=(9.35\pm0.35)\%$. The yield asymmetry was divided by the beam polarization to obtain the final PNC asymmetry of the *p*-wave resonances. These asymmetries are listed in Table I for all *p*-wave resonances observed in the present experiment. The table lists the resonance energy, the asymmetry of each *p*-wave resonance, and the asymmetry divided by its error. We consider as statistically significant those resonances with an asymmetry to uncertainty ratio of 3 or greater. Applying this 3σ criterion, there are four significant asymmetries in the present data. Only one of these cases, the 1.33-eV resonance with $p=(0.79\pm0.04)\%$, had been studied before with the following results: $p=(0.45\pm0.13)\%$ [1] and $p=(0.77\pm0.13)\%$ [32].

For the resonances with the most significant asymmetries

TABLE I. Measured longitudinal PNC asymmetries for neutron resonances in ^{117}Sn.

Energy (eV)	Asymmetry p (%)	$p/\Delta p$
1.33	0.786±0.036	21.7
15.39	-0.384±0.817	0.5
21.39	-0.044±0.662	0.1
26.22	0.279±0.154	1.8
34.04	-0.084±0.022	3.8
74.39	-0.003±0.033	0.1
158.33	0.018±0.035	0.5
166.32	0.686±0.656	1.0
200.78	-0.014±0.032	0.4
221.17	0.000±0.042	0.0
275.21	0.014±0.059	0.2
297.36	-0.028±0.039	0.7
423.29	-0.312±0.045	6.9
488.46	-1.315±0.577	2.3
526.34	-0.036±0.051	0.7
532.62	-0.007±0.042	0.2
554.57	0.008±0.064	0.1
573.24	-0.062±0.066	0.9
628.59	-0.052±0.293	0.2
646.68	0.030±0.060	0.5
658.50	0.054±0.046	1.2
685.74	0.037±0.067	0.6
694.43	-0.051±0.293	0.2
698.31	-0.075±0.104	0.7
852.58	0.055±0.126	0.4
882.31	-0.009±0.054	0.2
983.29	-0.037±0.176	0.2
1044.97	1.067±0.345	3.1
1078.56	0.116±0.243	0.5

(at 1.33 eV, 34.08 eV, and 423.3 eV, respectively), the data for the sum of the yields in the two neutron spin states are compared to the data for the difference in the yields in Figs. 1–3. The solid lines in the figures represent fits to the data: the FITXS fit to the sum of the yields and the difference of FITXS fits to the positive and negative yields. From the figure for the 1.33-eV resonance, one can infer the magnitude of the systematic errors in these data. For a large region of time of flight, the data on both sides of the resonance are consistent with zero difference, with small error bars. This consistency with zero difference is also displayed in the figures for the 34.08-eV and 423.3-eV resonances, although for smaller time-of-flight regions. The figure for the 423.3-eV resonance is interesting because it displays *s*-wave resonances along with the *p*-wave resonance. Even though there is a much larger count rate for the *s*-wave resonances, the difference between the yield for the two spin states is still very small.

IV. DETERMINATION OF WEAK SPREADING WIDTH

A likelihood analysis is performed to determine the weak mixing matrix element and the weak spreading width from the experimental asymmetries. Some of the *p*-wave resonances will display an asymmetry because of weak mixing between the *s*-wave and *p*-wave resonances, which occurs only between resonances with the same total spin *J*. For ^{117}Sn with target spin $I=\frac{1}{2}$, there are two sets of *s*-wave resonances ($J=0$ and 1) and three sets of *p*-wave resonances ($J=0$, 1, and 2). In this experiment, only a few of the *s*-wave resonances have known *J* values, and only the 1.33-eV *p*-wave resonance has a known spin $J=1$ [33].

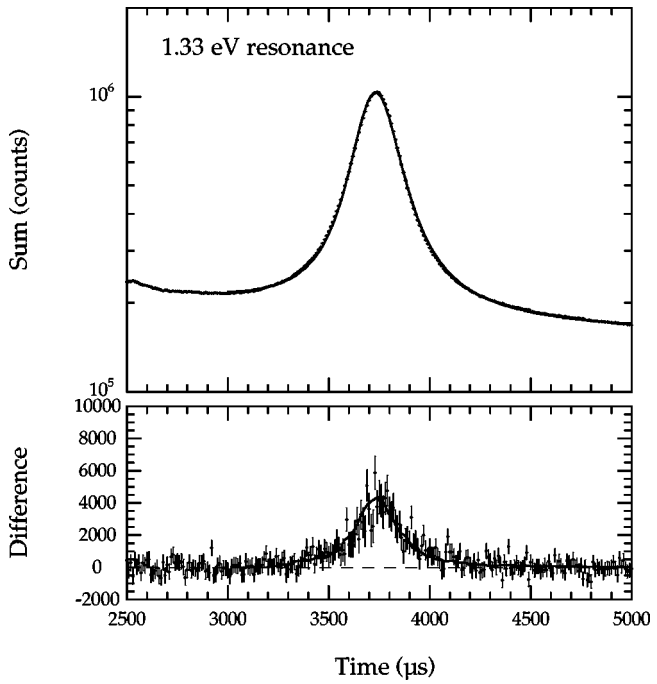

FIG. 1. Sum and difference data for the two neutron spin states in the region of the 1.33-eV resonance. The solid lines are fits to the data. These are the raw data before applying the polarization and multiscattering correction. The 1.33-eV resonance displays the most significant asymmetry measured in this work.

The analysis methods are discussed in detail by Bowman *et al.* [34]. The spirit of the approach is to include all available spectroscopic information and then to average over remaining unknown parameters. The magnitude of the parity violating asymmetry for a given *p*-wave resonance μ is given by

$$p_\mu = \sum_{\nu: J_\nu = J_\mu} \frac{2V_{\nu\mu}}{E_\mu - E_\nu} \frac{\sqrt{\Gamma_{\nu_n}}}{\sqrt{\Gamma_{\mu_n}}} \frac{g_{\mu_{1/2}}}{\sqrt{g^2_{\mu_{1/2}} + g^2_{\mu_{3/2}}}}, \qquad (1)$$

where the summation is over all *s*-wave resonances ν with $J_\nu = J_\mu$, $V_{\nu\mu}$ is the weak interaction matrix element, E_ν and E_μ are the energies of the *s*- and *p*-wave resonances, Γ_{μ_n} and Γ_{ν_n} are the corresponding neutron widths, and $g_{\mu_{1/2}}$ and $g_{\mu_{3/2}}$ are the projectile-spin neutron amplitudes ($g^2_{\mu_{1/2}} + g^2_{\mu_{3/2}} = \Gamma_{\mu_n}$). The weak interaction matrix element $V_{\nu\mu}$ is assumed

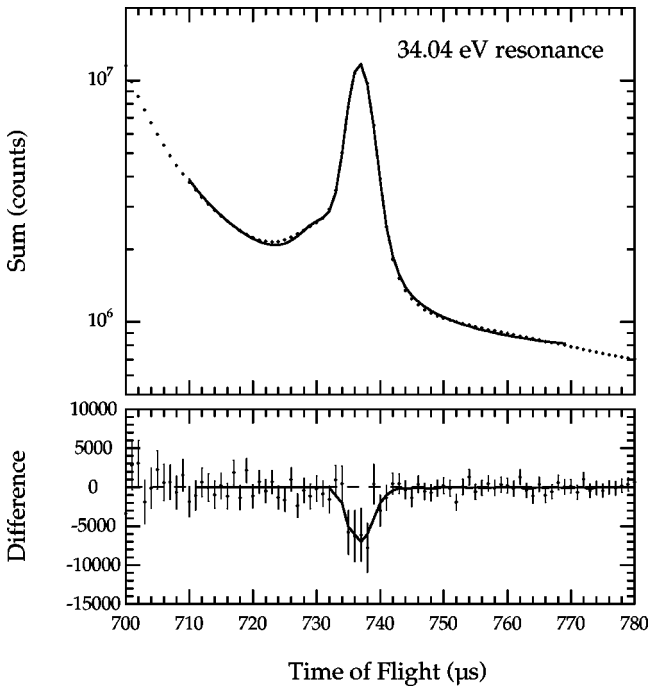

FIG. 2. Sum and difference data for the two neutron spin states in the region of the 34.04-eV resonance. The solid lines are fits to the data. The difference spectrum displays a statistically significant asymmetry.

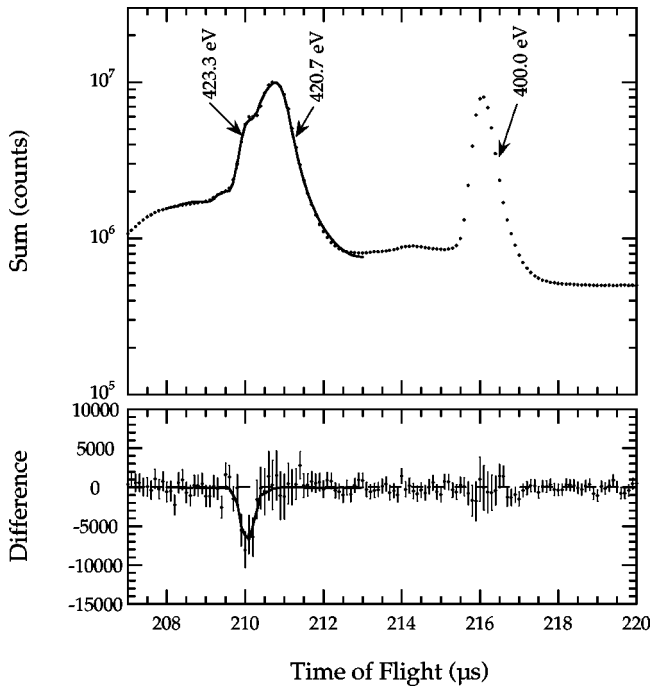

FIG. 3. Sum and difference data for the two neutron spin states in the region of the 423.3-eV resonance. The solid lines are fits to the data. The two *s*-wave resonances at 400.0 eV and 420.7 eV show no asymmetry in the difference data.

to be a Gaussian random variable with variance M^2. The probability density function for the asymmetry can then be written

$$P_p(p|MAR) = G(p, M^2A^2R^2). \tag{2}$$

The function G is a mean-zero Gaussian distribution of the variable p with a variance $M^2A^2R^2$, where A and R are

$$A_\mu^2 = \sum_{\nu: J_\nu = J_\mu} \left(\frac{2}{E_\mu - E_\nu}\right)^2 \frac{\Gamma_{\nu_n}}{\Gamma_{\mu_n}} \quad \text{and} \quad R = \frac{g_{\mu_{1/2}}}{\sqrt{g_{\mu_{1/2}}^2 + g_{\mu_{3/2}}^2}}. \tag{3}$$

The so-called enhancement factors $A = \sqrt{A_\mu^2}$ are determined from the resonance parameters. The amplitudes $g_{\mu_{1/2}}$ and $g_{\mu_{3/2}}$ are unknown, but are assumed to be Gaussian random variables. We define X^2 as the variance of $g_{1/2}$, and Y^2 the variance of $g_{3/2}$. The probability density functions of these quantities are Gaussian distributions,

$$P(g_{1/2}) = G(g_{1/2}, X^2) \quad \text{and} \quad P(g_{3/2}) = G(g_{3/2}, Y^2), \tag{4}$$

where X^2 and Y^2 can be related to the $S_{1/2}^1$ and $S_{3/2}^1$ *p*-wave strength functions. It is convenient to convert to polar coordinates $g_{1/2} = r \sin\theta$, $g_{3/2} = r \cos\theta$, and $R = \sin\theta$. After integration over r the probability density function becomes

$$P(\theta) = \frac{1}{2\pi} \frac{a}{a^2 \sin^2\theta + \cos^2\theta}, \tag{5}$$

where $a^2 = Y^2/X^2$ is the ratio of the $p_{3/2}$ to $p_{1/2}$ strength functions. The final probability density function for the measured asymmetry is

$$P_p^l(p|MA, a, \sigma) = \frac{2}{\pi} \int_0^{\pi/2} \frac{a}{a^2 \sin^2\theta + \cos^2\theta} G(p, M^2A^2 \sin^2\theta + \sigma^2) d\theta, \tag{6}$$

where p is the magnitude and σ the experimental error of the asymmetry.

The asymmetries and their errors were determined in the present experiment, the neutron widths and energies were determined previously by our group [31], and the ratio a^2 had been measured earlier [35]. We therefore are able to formulate the probability density function for each *p*-wave resonance. However, since the J values of the *p*-wave resonances are unknown, one does not know which set of *s*-wave resonances mix to cause parity violation. There are three sets of *p*-wave resonances, and one can form the probability density function for each of the three spin states. The relative probability of the resonance to have a particular J value is estimated from a general statistical argument and these three probability density functions combined. Since there are two sets of *s*-wave resonances, there are two different weak mix-

TABLE II. Resonance parameters for parity violation analysis in ^{117}Sn (for a definition of $A_{J_p}^{J_s}$, see text).

Energy (eV)	J	l	$g\Gamma_n$ (meV)	A_0^1 (eV^{-1})	A_1^1 (eV^{-1})	A_0^0 (eV^{-1})	A_1^0 (eV^{-1})
−29.2	1	0	30.0				
1.327±0.001	1	1	0.000138±0.000007		11.10		11.05
15.385±0.016		1	0.000092±0.000005	1.98	20.8	3.03	20.7
21.390±0.025		1	0.000206±0.000011	1.50	16.26	2.25	16.17
26.215±0.034		1	0.00207±0.00010	0.52	6.50	0.76	6.47
34.044±0.017		1	0.0187±0.0009	0.20	5.34	0.28	5.33
38.8 ±0.05	1	0	3.10±0.15				
74.39±0.04		1	0.034±0.002	0.29	1.01	0.36	0.99
120.54±0.06	1	0	4.95±0.25				
123.90±0.07	0	0	2.1±0.1				
158.33±0.09		1	0.0025±0.0001	1.84	4.80	2.17	4.67
166.32±0.09		1	0.160±0.008	0.19	0.68	0.25	0.66
196.20±0.11	1	0	12.2±0.6				
200.78±0.12		1	0.48±0.02	0.08	2.23	0.13	2.23
221.17±0.13		1	0.22±0.01	0.11	0.67	0.21	0.66
275.21±0.17		1	0.17±0.01	0.13	0.52	0.38	0.37
297.36±0.18		1	0.43±0.02	0.08	0.40	0.33	0.23
341.63±0.22		0	15.9±0.8				
357.60±0.23		0	12.0±3.5				
400.03±0.27		0	3.7±0.2				
420.73±0.28	1	0	62.5±7.5				
423.29±0.28		1	1.55±0.08	0.16	4.97	0.25	4.97
458.99±0.32	0	0	12.5±1.5				
488.46±0.34		1	0.036±0.002	1.42	1.46	1.55	1.33
526.34±0.38		1	0.96±0.07	0.23	0.21	0.25	0.18
532.62±0.38		1	1.46±0.10	0.20	0.16	0.22	0.14
554.57±0.40		1	0.74±0.06	0.49	0.21	0.50	0.17
573.24±0.42		1	0.78±0.06	1.63	0.19	1.64	0.15
580.8±1.0	0	0	30±3				
628.59±0.47		1	0.141±0.013	0.64	0.45	0.71	0.33
646.68±0.49		1	1.20±0.12	0.17	0.16	0.20	0.12
658.50±0.50		1	2.2±0.2	0.11	0.12	0.14	0.09
685.74±0.53		1	1.15±0.12	0.18	0.19	0.22	0.14
694.43±0.54		1	0.19±0.02	0.69	0.48	0.77	0.35
698.31±0.54		1	0.72±0.08	0.53	0.25	0.56	0.18
705.76±0.55		(0)	2.6±0.3				
789.41±0.64		0	11.0±1.3				
812.92±0.66	1	0	65±6				
852.58±0.71		1	0.79±0.10	0.06	0.83	0.69	0.47
864.51±0.72		0	10.5±2.1				
882.31±0.74		1	3.6±0.5	0.03	0.30	0.27	0.13
939.22±0.80		0	20±2				
983.29±0.85		1	0.92±0.13	0.04	5.1	5.10	0.12
989.37±0.86		0	200±30				
996.13±0.87		0	90±15				
1044.97±0.93		1	0.42±0.06	0.05	1.04	1.03	0.16
1078.56±0.97		1	0.66±0.10	0.04	0.54	0.53	0.12

ing matrix elements for $J=0$ and for $J=1$. We assume that these two matrix elements differ in strength only because of the difference in s-wave level density for the two J values. We therefore define the weak spreading width,

$$\Gamma_w = \frac{2\pi M_J^2}{D_0(J)}, \tag{7}$$

where M_J is the J-dependent weak mixing matrix el-

ement and $D_0(J)$ is the average *s*-wave level spacing for each total spin *J*. The weak spreading width is assumed to be independent of *J*. Therefore one fits directly to the weak spreading width.

To resolve the normalization issue, we assume that the prior probability density function $P_{\Gamma_w}(\Gamma_w)$ is one up to a value of $\Gamma_{w,max}$ and zero above this value. The likelihood function for a *p*-wave resonance μ can now be written as

$$L_\mu(\Gamma_w)=P_{\Gamma_w}(\Gamma_w)\left(\sum_{J=0,1} p(J)P_p(p|M_J,A_\mu(J),a,\sigma) + \sum_{J=2} p(J)G(p,\sigma^2)\right). \quad (8)$$

The function $p(J)$ is the relative probability for a *p*-wave resonance to have total spin *J*, and M_J is the matrix element that corresponds to the weak spreading width Γ_w. The total likelihood function is the product of the individual likelihood functions for each *p*-wave resonance. The errors on Γ_w are given by

$$\ln\left[\frac{L(\Gamma_w^{\pm})}{L(\Gamma_w^*)}\right]=-\frac{1}{2}, \quad (9)$$

where Γ_w^* is the most likely value and $\Gamma_w^{\pm}$ gives the confidence range. The relative probability $p(J)$ is found from the spin distribution, which can be approximated by

$$f(J)=\frac{2J+1}{2\sigma_c^2}e^{[-(J+1/2)^2]/2\sigma_c^2}, \quad (10)$$

where *J* is the total spin, and σ_c is the spin cutoff parameter

$$\sigma_c=(0.98\pm0.23)A^{(0.29\pm0.06)}, \quad (11)$$

which was determined empirically by fitting to nuclei from $A=20$ to 250 [36]. The probability $p(J)$ is found by normalizing the sum of $f(J)$ to 1.

Another difficulty is the absence of complete information on the *J* values of the *s*-wave resonances that are necessary for the calculations of the amplification parameters A_μ, Eq. (3). For many of the *s*-wave resonances the *J* values were determined in earlier measurements. Most importantly for this measurement is that the *J* values are known for most of the low energy *s*-wave resonances that are near the *p*-wave resonances, which display significant asymmetries. Since the PNC effect is inversely proportional to the energy difference between the *s*-wave and *p*-wave resonances, these are the most important. As a way to estimate the magnitude of the effect on the weak spreading width due to this lack of information, we made two extreme assumptions: the unknown spins of *s*-wave resonances were assumed to be all $J=0$ or all $J=1$. These two options are presented by four $A_{J_p}^{J_s}$ columns in Table II. The upper index in $A_{J_p}^{J_s}$ refers to the assumption of $J=0$ or $J=1$ for *s*-wave resonances with unknown spins. The likelihood analyses for these two extreme assumptions should bracket the true best value and also provide an estimate of the uncertainty introduced due to this lack of information.

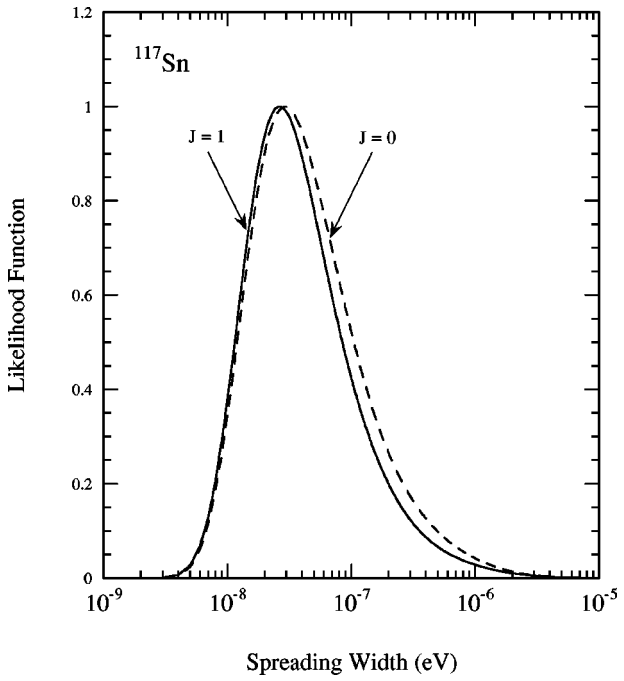

FIG. 4. The likelihood functions calculated from the asymmetry data in ^{117}Sn. For both curves the maximum likelihood has been normalized to one. The two curves were generated under two extreme assumptions: that the spins of all of the *s*-wave resonances with unknown spins are either $J=0$ or $J=1$. These two curves represent extreme assumptions that should bracket the true likelihood curve.

The resulting likelihood curves are shown in Fig. 4. Since most of the *s*-wave resonances near the *p*-wave resonances with significant PNC effects have a known spin, the difference between the most likely weak spreading widths under these two extreme assumptions is small. The final value of the weak spreading width is the average of these two values, $\Gamma_w = (0.28^{+0.56}_{-0.15})\times10^{-7}$ eV. This value replaces a previously published one from a preliminary analysis of this data set [6]. The previously stated number did not use new values for resonance parameters [31] and used online spectra without further data cuts or polarization calibration.

V. DISCUSSION OF WEAK SPREADING WIDTH

The measured value for the weak spreading width in ^{117}Sn is an order of magnitude smaller than in nearby nuclei ($2.56^{+0.83}_{-0.63}\times10^{-7}$ eV, a local average from ^{93}Nb, ^{103}Rh, ^{107}Ag, ^{109}Ag, ^{113}Cd, ^{121}Sb, ^{123}Sb, ^{127}I, and ^{133}Cs) [12]. The smallness of the weak spreading width in ^{117}Sn has a natural explanation in terms of the structure of matrix elements of the weak interaction in the theory of Tomsovic, Johnson, Hayes, and Bowman [37], who have described the weak strength function within the framework of statistical spectroscopy. In this theory, the weak strength function is expressed in terms of sums of squares of matrix elements of the effective weak potential between two-nucleon configura-

TABLE III. Square of the weak mixing matrix elements for Pd isotopes for $F_0=F_\pi=10^{-6}$. These values are an example of configuration strengths in this mass region. For ^{117}Sn there is a closed proton shell, and hence only the *n*-*n* configuration can produce the observed parity violation.

Configuration	π meson (eV^2)	ρ meson (eV^2)
n-*p*	0.64	0.022
p-*p*	0.0019	0.024
n-*n*	5.6×10^{-5}	0.0032

tions weighted by functions that change smoothly with *N*, *Z*, and *A*. The configurations involved are in the $0\hbar\omega$ space of the nuclear system—those configurations that can be reached from the ground state without promoting a nucleon across a major shell.

In Table III we show the square of weak matrix elements averaged over available two-body configurations for Pd isotopes (representative of the mass 100 region of nuclei). The interaction is built up from exchanges of mesons, with the results in Table III containing just the (important) weak $\Delta I=1$ π-nucleon and $\Delta I=0$ ρ-nucleon couplings; 1-$\hbar\omega$ excitations out of the model space are accounted for by a ''doorway'' term added to the interaction. The largest entry in Table III is for the *n*-*p* configuration, which is dominated by the exchange of the longest-range piece of the interaction, the π meson; the small nonvanishing entry for the *n*-*n* and *p*-*p* configurations also arises from the pion, in this case mediated by the core in the doorway term.

For the Pd isotopes, both neutron and proton orbitals are active, so the weak spreading width is dominated by the large *n*-*p* matrix elements. However, for ^{117}Sn, neither *n*-*p* nor *p*-*p* configurations contribute to the weak spreading width because this nucleus has a closed proton shell, and the weak spreading width is given by the much smaller *n*-*n* matrix elements. Table III would suggest a weak spreading width about an order of magnitude smaller than for nearby nuclides. Additionally, one sees that this nucleus is dominated by the coupling to the ρ meson, so that ^{117}Sn may be the best case for determining the weak ρ-nucleon coupling.

The fact that the measured weak spreading width in ^{117}Sn is dominated by F_0 and is an order of magnitude smaller than for nearby nuclides cannot in itself be used to determine F_0 short of a calculation with the full machinery of statistical spectroscopy. (We may nevertheless obtain an estimate by normalizing to our earlier calculation in the Pd isotopes [37], obtaining F_0 near the upper limit allowed by the Desplanques, Donoghue, and Holstein (DDH) analysis [3].) However, the smallness of the weak spreading width for ^{117}Sn relative to nearby nuclides does confirm the very general prediction of the model of Tomsovic, Johnson, Hayes, and Bowman and was in fact the original motivation for measurements with this target. If the measured weak spreading width for ^{117}Sn had been comparable to neighboring nuclides, no adjustments of the coupling constants could have explained that outcome, and this apparent discrepancy with statistical spectroscopy would have been suggestive of some unexpected or unaccounted physics at work in ^{117}Sn.

VI. SUMMARY

The longitudinal asymmetries of neutron *p*-wave cross sections were measured for 29 resonances in ^{117}Sn in the neutron energy region from 0.8 to 1100 eV. Analysis of these asymmetries was performed using the neutron resonance parameters recently determined by the TRIPLE Collaboration [31]. Statistically significant parity violating asymmetries were observed in the neutron resonances at 1.33, 34.04, 423.3, and 1045.0 eV. All measured asymmetries for *p*-wave resonances observed below 490 eV were used in a likelihood analysis to find the weak spreading width. The value $\Gamma_w=(0.28^{+0.56}_{-0.15})\times10^{-7}$ eV is 2σ below the average value for the weak spreading width in this mass region [12]. This loss in strength of the weak spreading width can be explained by the theory of statistical spectroscopy [37].

ACKNOWLEDGMENTS

This work was supported in part by the U.S. Department of Energy, Office of High Energy and Nuclear Physics, under Grant Nos. DE-FG02-97-ER41042 and DE-FG02-97-ER41033, and by the U.S. Department of Energy, Office of Energy Research, under Contract No. W-7405-ENG-36.

[1] V. P. Alfimenkov, S. B. Borzakov, Vo Van Thuan, Yu. D. Mareev, L. B. Pikelner, A. S. Khrykin, and E. I. Sharapov, Nucl. Phys. **A398**, 93 (1983).
[2] O. Sushkov and V. V. Flambaum, JETP Lett. **32**, 352 (1980).
[3] E. G. Adelberger and W. C. Haxton, Annu. Rev. Nucl. Part. Sci. **35**, 501 (1985).
[4] J. D. Bowman, G. T. Garvey, Mikkel B. Johnson, and G. E. Mitchell, Annu. Rev. Nucl. Part. Sci. **43**, 829 (1993).
[5] V. V. Flambaum and G. F. Gribakin, Prog. Part. Nucl. Phys. **35**, 423 (1995).
[6] G. E. Mitchell, J. D. Bowman, and H. A. Weidenmüller, Rev. Mod. Phys. **71**, 445 (1999).
[7] J. D. Bowman *et al.*, Phys. Rev. Lett. **65**, 1192 (1990).
[8] C. M. Frankle *et al.*, Phys. Rev. Lett. **67**, 564 (1991).
[9] B. E. Crawford *et al.*, Phys. Rev. C **58**, 1225 (1998).
[10] S. L. Stephenson *et al.*, Phys. Rev. C **58**, 1236 (1998).
[11] E. I. Sharapov *et al.*, Phys. Rev. C **59**, 1131 (1999).
[12] D. A. Smith *et al.*, Phys. Rev. C **60**, 045503 (1999).
[13] B. E. Crawford *et al.*, Phys. Rev. C **60**, 055503 (1999).
[14] L. Y. Lowie *et al.*, Phys. Rev. C **59**, 1119 (1999).
[15] S. J. Seestrom *et al.*, Phys. Rev. C **58**, 2977 (1998).
[16] S. L. Stephenson *et al.*, Phys. Rev. C **61**, 045501 (2000).
[17] Y. Matsuda, Ph.D. thesis, Kyoto University, Report No. KUNS 1492, 1998.
[18] E. I. Sharapov *et al.*, Phys. Rev. C **59**, 1772 (1999).
[19] P. W. Lisowski, C. D. Bowman, G. J. Russell, and S. A.

Wender, Nucl. Sci. Eng. **106**, 208 (1990).
[20] C. M. Frankle, J. D. Bowman, S. J. Seestrom, N. R. Roberson, and E. I. Sharapov, in *Time Reversal Invariance and Parity Violation in Neutron Resonances*, edited by C. R. Gould, J. D. Bowman, and Yu. P. Popov (World Scientific, Singapore, 1994), p. 204.
[21] S. J. Seestrom *et al.*, Nucl. Instrum. Methods Phys. Res. A **433**, 603 (1999).
[22] B. E. Crawford, J. D. Bowman, S. I. Penttilä, and N. R. Roberson, Nucl. Instrum. Methods Phys. Res. A (to be published).
[23] J. J. Szymanski *et al.*, Nucl. Instrum. Methods Phys. Res. A **340**, 564 (1994).
[24] S. I. Penttila, J. D. Bowman, P. P. J. Delheij, C. M. Frankle, D. G. Haase, R. Mortensen, H. Postma, S. J. Seestrom, and Yi-Fen Yen, in *Time Reversal Invariance and Parity Violation in Neutron Resonances*, edited by C. R. Gould, J. D. Bowman, and Yu. P. Popov (World Scientific, Singapore, 1994), p. 198.
[25] S. I. Penttila, J. D. Bowman, P. P. J. Delheij, C. M. Frankle, D. G. Haase, H. Postma, S. J. Seestrom, and Yi-Fen Yen, in *High Energy Spin Physics*, edited by Kenneth J. Heller and Sandra L. Smith, AIP Conf. Proc. No. 34 (AIP, Woodbury, NY, 1995), p. 532.
[26] J. D. Bowman, S. I. Penttila, and W. B. Tippens, Nucl. Instrum. Methods Phys. Res. A **369**, 195 (1996).
[27] V. W. Yuan *et al.*, Phys. Rev. C **44**, 2187 (1991).
[28] B. E. Crawford *et al.*, in *VI International Seminar on Interaction of Neutrons with Nuclei*, JINR Report No. E3-96-336 (Joint Institute for Nuclear Research, Dubna, 1996), p. 268.
[29] J. D. Bowmam, Y. Matsuda, Y.-F. Yen, and B. E. Crawford (unpublished).
[30] C. W. Reich and M. S. Moore, Phys. Rev. **111**, 929 (1958).
[31] D. A. Smith *et al.*, Phys. Rev. C **59**, 2836 (1999).
[32] S. A. Biryukov *et al.*, Yad. Fiz. **45**, 1511 (1987) [Sov. J. Nucl. Phys. **45**, 937 (1987)].
[33] V. P. Alfimenkov, S. B. Borzakov, Vo Van Thuan, Yu. D. Mareev, L. B. Pikelner, I. M. Frank, A. S. Khrykin, and E. I. Sharapov, Pis'ma Zh. Eksp. Teor. Fiz. **39**, 416 (1984) [JETP Lett. **39**, 416 (1984)].
[34] J. D. Bowman, L. Y. Lowie, G. E. Mitchell, E. I. Sharapov, and Yi-Fen Yen, Phys. Rev. C **53**, 285 (1996).
[35] A. B. Popov and G. S. Samosvat, Sov. J. Nucl. Phys. **45**, 944 (1987).
[36] T. von Egidy, H. H. Schmidt, and A. N. Behkami, Nucl. Phys. **A451**, 189 (1998).
[37] S. Tomsovic, M. B. Johnson, A. Hayes, and J. D. Bowman, Phys. Rev. C **62**, 054607 (2000).